Pezhman Akbari
Department of Mechanical Engineering,
Michigan State University,
2500 Engineering Building,
East Lansing, MI 48824-1226
e-mail: akbari@egr.msu.edu

Razi Nalim
Department of Mechanical Engineering,
Indiana University–Purdue University
Indianapolis (IUPUI),
Indianapolis, IN 46202-5132
e-mail: mnalim@iupui.edu

Norbert Müller
Department of Mechanical Engineering,
Michigan State University,
2455 Engineering Building,
East Lansing, MI 48824-1226
e-mail: Mueller@egr.msu.edu

Performance Enhancement of Microturbine Engines Topped With Wave Rotors

Significant performance enhancement of microturbines is predicted by implementing various wave-rotor-topping cycles. Five different advantageous cases are considered for implementation of a four-port wave rotor into two given baseline engines. In these thermodynamic analyses, the compressor and turbine pressure ratios and the turbine inlet temperatures are varied, according to the anticipated design objectives of the cases. Advantages and disadvantages are discussed. Comparison between the theoretic performance of wave-rotor-topped and baseline engines shows a performance enhancement up to 34%. General design maps are generated for the small gas turbines, showing the design space and optima for baseline and topped engines. Also, the impact of ambient temperature on the performance of both baseline and topped engines is investigated. It is shown that the wave-rotor-topped engines are less prone to performance degradation under hot-weather conditions than the baseline engines. [DOI: 10.1115/1.1924484]

Introduction

A growing market for distributed power generation and propulsion of small vehicles has motivated a strong interest in design of small gas turbine systems in the range of 30–300 kW. Known as microturbines, they are now widely used in the US for distributed power generation, shaving peak loads, and providing backup power for critical needs. They propel small commercial aircraft, unmanned air vehicles (UAV), and terrestrial vehicles. Microturbines are often the preferred alternative to IC engines, because of their higher power density and robustness. They present several advantageous features such as compact size, simple operability, ease of installation, low maintenance, fuel flexibility, and low NO_X emissions. Furthermore, recent electric-power crises and environmental concerns have stimulated a strong interest in the research, development, and application of microturbines.

Despite their attractive features, compared with larger gas turbines, microturbines suffer from lower thermal efficiency and their relative output power, due to their (lower) component efficiencies, limited cycle pressure ratio, and peak cycle temperature. For example, experimental and theoretical research has shown that microturbines with pressure ratios of 3–5 without recuperation systems achieve only about 15%–20% efficiency [1,2]. For many applications improvement of their performance is desirable to enhance advantages over competing technologies. To achieve such improvements, current efforts are mainly focused on utilizing heat recovery devices, developing new high-strength, high-temperature materials for turbine blades, and improving the aerodynamic quality of turbomachinery components [3]. The aerodynamics of turbomachinery has already yielded very high component efficiencies up to around 90% [4]. Further improvement is possible, but huge gains seem unlikely especially for small compressors with unavoidable tip leakage. Geometries of microturbines make blade cooling very difficult and internal cooling methods applied to larger engines are often impractical for smaller turbines. Hence, their lifetimes are shorter when using materials typical of larger gas turbines [5]. Therefore, there is significant research toward developing advanced metallic alloys and ceramics for high-thermal-resistance turbine wheels used in microturbines [6,7]. Utilizing conventional recuperators based on the use of existing materials can improve the overall efficiency of microturbines up to 30% [2,8–10]. Despite the attractive feature of the recuperator concept, a recuperator adds about 25%–30% to the overall engine manufacturing cost, which is a challenge for commercialization of microturbines [11–13]. The current trend of the microturbine market is to reduce the investment cost. Therefore, alternative devices need to be considered to achieve higher performance at lower component costs. Topping a microturbine with a wave rotor device is an appropriate solution.

In a wave-rotor-topped cycle, the combustion can take place at a higher temperature while the turbine inlet temperature can be equal to that of the baseline cycle. Also, a pressure gain additional to that provided by the compressor is obtained by the wave rotor. Thus, the wave rotor can increase the overall pressure ratio and peak cycle temperature beyond the limits of ordinary turbomachinery. The performance enhancement is achieved by increasing both thermal efficiency and output work, hence reducing specific fuel consumption rate considerably. This enhancement is especially favorable for smaller gas turbines often used for distributed power generation or propulsion of small vehicles [14–17].

Wave Rotor History. The first successful wave rotor was tested by Brown Boveri Company (BBC), later Asea Brown Boveri (ABB), in Switzerland in the beginning of the 1940s [18] as a topping stage for a locomotive gas turbine engine [19–22], based on the patents of Seippel [23–26]. This first unit suffered from inefficient design and crude integration [21]. Later, BBC focused on the development of pressure wave superchargers for diesel engines, anticipating greater payoff [27]. By 1987, their Comprex® supercharger appeared in the Mazda 626 Capella passenger car [28,29]. Since then, the Comprex® has been commercialized for heavy diesel engines, and also tested successfully on vehicles such as Mercedes-Benz [30], Peugeot, and Ferrari [27]. Such a pressure-wave supercharger offers rapid load response and scale-independent efficiency, making its light weight and compact size attractive for supercharging small engines (below about 75 kW or 100 hp) [31,32].

Propulsion applications resumed in the 1960s, with General Electric Company (GE), General Power Corporation (GPC), Mathematical Science Northwest (MSNW), and Rolls Royce developing prototypes [27,33]. In the 1980s, US agencies like the Defense Advanced Research Projects Agency (DARPA) and the Navy sponsored research programs on wave rotor science and

Contributed by the IGTI Microturbines and Small Turbomachinery Committee of the ASME for publication in the JOURNAL OF ENGINEERING FOR GAS TURBINES AND POWER. Manuscript received March 12, 2004; final manuscript received December 13, 2004. Committee Chair: D. Haught.

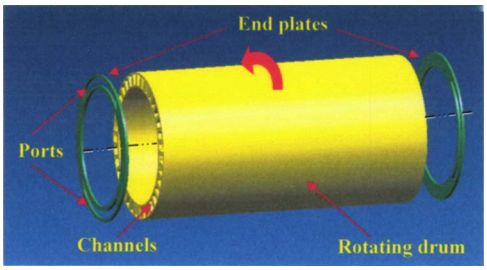

Fig. 1 Schematic configuration of a typical wave rotor

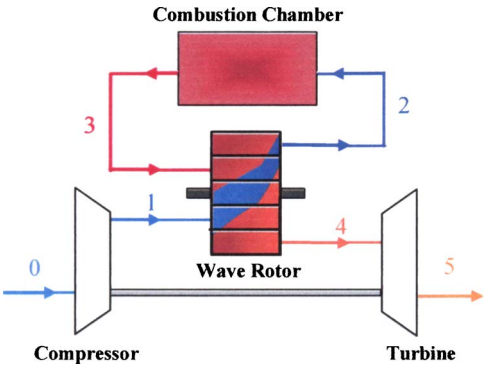

Fig. 2 Schematic of a gas turbine topped by a four-port wave rotor

technology. The 1985 ONR/NAVAIR Wave Rotor Research and Technology Workshop [33] offered a comprehensive review of prior work.

Since the late 1980s, a sustained research program at NASA Glenn Research Center (GRC) collaborating with the US Army Research Laboratory (ARL) and Rolls-Royce Allison has aimed to develop and demonstrate the benefits of wave rotor technology for future aircraft propulsion systems [34–40]. Experimental studies at NASA on four-port [41] and three-port [42–44] wave rotors enabled the estimation of loss budgets [45,46] and simulation code validation [47]. Initially, a simple three-port flow divider wave rotor was built and tested to evaluate loss mechanisms and calibrate the simulation code. Next, a four-port pressure exchanger was built and was tested to evaluate the pressure-gain performance for application to a small gas turbine (Allison 250). Wave rotor cycles with lower thermal loads have been proposed [48,49], and mechanical design issues are being addressed in current NASA-sponsored research.

The French National Aerospace Research Establishment (ONERA) has also investigated wave rotor enhancement of gas turbines in auxiliary power units, turboshaft, turbojet, and turbofan engines [15]. Consistent with NASA studies [50], ONERA anticipates the largest gains and efficiency for engines with a low compressor pressure ratio and high turbine inlet temperature, such as turboshaft engines and auxiliary power units.

The objective of the present work is a comprehensive and systematic performance analysis of two actual microturbines known as the C-30 and C-60 engines which are topped with a four-port wave rotor in various wave-rotor-topping cycles. The challenges and advantages associated with the different implementation cases are discussed. While the performance evaluation of several gas turbine engines has been studied extensively [14,15,50], to the knowledge of the author, there exits no comprehensive work investigating the potential benefits of various implementation cases of wave rotor topping cycles for small gas turbines. The presented results have been obtained using basic thermodynamic equations along with the wave-rotor characteristic equation previously validated using computational tools [14]. The model can be employed to predict the performance improvement of various wave-rotor-topping cycles without the need for knowing the details of the complex fluid mechanics within the wave rotor.

Wave Rotor Description

Wave rotors do not use mechanical components such as pistons or vaned impellers to compress the fluid. Instead, the pressure rise is obtained by generating compression waves in appropriate geometries. It has been proven that for the same inlet and outlet Mach numbers the pressure gain in time-dependent flow devices can be much greater than in steady flow devices [51–53].

The essential feature of wave rotors is an array of channels arranged around the axis of a cylindrical drum. As schematically shown in Fig. 1, the drum rotates between two end plates each of which has a few ports or manifolds, controlling the fluid flow through the channels. The number of ports and their positions vary for different applications. By carefully selecting their locations and widths to generate and utilize wave processes, a significant and efficient transfer of energy can be obtained between flows in the connected ducts. Through rotation, the channel ends are periodically exposed to the ports located on the stationary end plates initiating compression and expansion waves within the wave rotor channels. Thus, pressure is exchanged dynamically between fluids by utilizing unsteady pressure waves. Unlike a steady-flow turbomachine that either compresses or expands the fluid, the wave rotor accomplishes both compression and expansion within a single component. Even though the wave rotor is internally unsteady, the flows in the ports are almost steady, aside from the fluctuations due to the opening and closing of the channels as they enter and exit port regions. Therefore, the wave rotor outflow shows very low pulsating behavior. To minimize leakage, the gap between the end plates and the rotor has to be very small, but without contact under all operating and thermal expansion conditions.

With axial channels and matched port flow alignment, the power required to keep the rotor at a correctly designed speed is negligible [54,55]. It only needs to overcome rotor windage and friction. In such a configuration, the rotor may be gear or belt driven or preferably direct driven by an electrical motor (not shown). Alternatively, a self-driving configuration, known as the "free-running rotor," can drive itself by using port flow incidence on channel walls to turn the rotor [28,30].

In a conventional arrangement, the wave rotor is embedded between the compressor and turbine "parallel" to the combustion chamber. Figure 2 illustrates how a four-port wave rotor is used to top an unrecuperated (simple) gas turbine cycle. Figure 3 schematically shows how the wave rotor could be embedded physically into an unrecuperated baseline engine that uses single-stage radial compressor and turbine. Two practical design arrangements of installation of a four-port wave rotor in such a gas turbine engine are described in detail in Ref. [56].

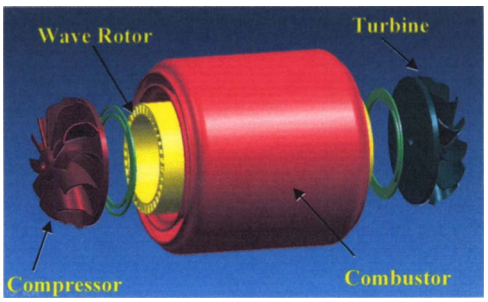

Fig. 3 Schematic example of the physical implementation of a wave rotor in a gas turbine (exploded view, piping not shown)

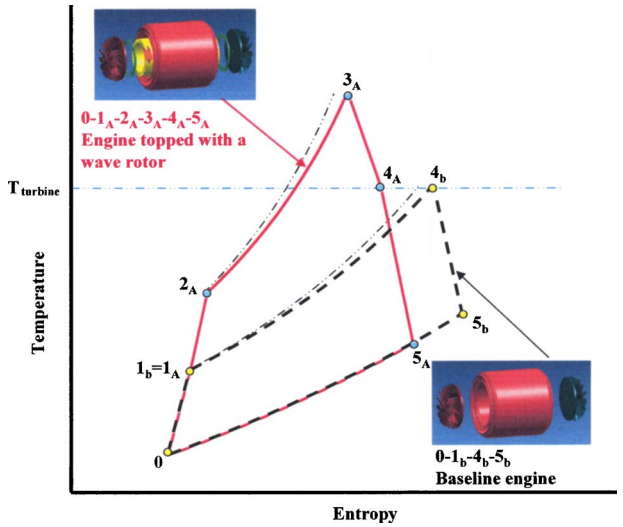

Fig. 4 Schematic T-s diagrams for a gas turbine baseline engine and the most common implementation case of a topping wave rotor

Following the flow path shown in Fig. 2, air from the compressor enters the wave rotor (state 1) and is further compressed inside the wave rotor channels. After the additional compression of the air in the wave rotor, it discharges into the combustion chamber (state 2). The hot gas leaving the combustion chamber (state 3) enters the wave rotor and compresses the air received from the compressor (state 1). To provide the energy transfer to compress the air, the burned gas partially expands in the wave rotor en route to the turbine (state 4). Due to the pre-expansion in the wave rotor, the burned gas enters the turbine with a lower temperature than that of the combustor exit. However, the turbine inlet total pressure is typically 15%–20% higher than the air pressure delivered by the compressor [40]. This pressure gain is in contrast to the untopped engine, where the turbine inlet pressure is always lower than the compressor discharge pressure, due to the pressure loss across the combustion chamber. As a result of the wave rotor pressure gain, more work can be extracted from the turbine increasing engine thermal efficiency and specific work. Finally, the channels are re-connected to the compressor outlet, allowing fresh pre-compressed air to flow into the wave rotor channels and the cycle repeats.

The general advantage of using a wave rotor becomes apparent when comparing the thermodynamic cycles of baseline and wave-rotor-enhanced engines. Figure 4 shows schematic T-s diagrams of the baseline engine and the corresponding wave-rotor-topped engine. The shown wave rotor implementation is the one most commonly discussed in references, referred to as Case A in this study. It is evident that both gas turbines are operating with the same turbine inlet temperature and compressor pressure ratio. Each wave rotor investigated in this work has zero shaft work. Therefore, the wave rotor compression work is equal to the wave rotor expansion work. Thus, the energy increase from state "1_b" to "4_b" in the baseline engine and from state "1_A" to "4_A" in the wave-rotor-topped engine is the same. This results in the same heat addition for both cycles. However, the output work of the topped engine is higher than that of the baseline engine due to the pressure gain across the wave rotor ($p_{t4A} > p_{t4b}$, where subscript "t" indicates total values). Therefore, the thermal efficiency for the topped engine is higher than that of the baseline engine. The inherent gas dynamic design of the wave rotor compensates for the combustor pressure loss from state "2_A" to "3_A," meaning that the compressed air leaving the wave rotor is at higher pressure than the hot gas entering the wave rotor.

There are several other important advantages of wave rotor machines. Their rotational speed is low compared with turbomachines, which results in low material stresses. They can respond on the time scale of pressure waves with no rotor inertial lag. From a mechanical point of view, their geometries can be simpler than those of turbomachines. Therefore, they can be manufactured relatively inexpensively. Also, the rotor channels are less prone to erosion damage than the blades of turbomachines. This is mainly due to the lower velocity of the working fluid in the channels, which is about one-third of what is typical within turbomachines [55]. Another important advantage of wave rotors is their self-cooling capabilities. In heat engine applications, the rotor channels pass both air (being compressed) and hot gas (being expanded) in the cycle at least once per rotor revolution, alternating faster than thermal diffusion rates. The rotor temperature equilibrates between the temperature of the cooler air and the hotter gas, allowing peak cycle temperature above materials limits.

Table 1 Baseline engine data, assuming T_0=300 K, Cp_{air} =1.005 kJ/kgK, Cp_{gas}=1.148 kJ/kgK, γ_{air}=1.4, γ_{gas}=1.33

Baseline engine		C-30	C-60
turbine inlet temperature	T_{t4b}	1116.5 K (1550° F)	1227.6 K (1750° F)
compressor outlet temperature	T_{t1b}	466.5 K (380° F)	505.4 K (450° F)
compressor pressure ratio	p_{t1b}/p_0	3.6	4.8
compressor isentropic efficiency	η_C	79.6%	82.6%
turbine isentropic efficiency	η_T	84%	85%
compressor polytropic efficiency	η_{PC}	82.9%	85.9%
turbine polytropic efficiency	η_{PT}	81.7%	82.3%

Thermodynamic Calculations

To evaluate the performance enhancement of topping small gas turbines with wave rotors, a computer program based on a thermodynamic approach was created to determine the thermodynamic properties of the gases in different states of the cycles. The results are used to calculate the theoretical performance (expressed by specific cycle work w, thermal efficiency η, and specific fuel consumption SFC) and the actual T-s diagrams of both wave-rotor-topped and baseline engines. The methodology is similar to that introduced by Wilson and Paxson [14] with some modifications.

For thermodynamic calculations, two unrecuperated microturbine engines called C-30 and C-60 made by Capstone Turbine Corporation are considered here. The component performance parameters for the baseline engines are based on information provided by the manufacturer and are listed in Table 1. For each engine it is assumed that the compressor inlet condition is known and is the same for both baseline and wave-rotor-enhanced engines. Considering the same "aerodynamic quality" of the wheels, the polytropic efficiencies are kept the same for the enhanced and baseline engine, for the compressor and turbine, respectively. Incomplete combustion of the fuel is reflected by a combustor efficiency of 98% (η_Q=0.98). Also a 2% pressure drop in the combustion chamber is considered (Π_{comb}=0.98). Air enters the compressor at 300 K. For both air and burned gas constant values of specific heat coefficients (Cp_{air}=1.005 kJ/kgK, Cp_{gas} =1.148 kJ/kgK) and specific heat ratios (γ_{air}=1.4, γ_{gas}=1.33) are considered. This assumption simplifies the performance calculations significantly without affecting the qualitative nature of the results. Consistently with previous wave rotor investigations [14,15,57], the wave rotor compression and expansion efficiencies are assumed as $\eta_{WC}=\eta_{WE}$=0.83. These efficiencies take into account irreversible effects such as friction. In addition, a wave rotor compression ratio of $PR_W=p_{t2}/p_{t1}$=1.8 appears to be conceivable for the envisioned application [14,15,57] and is chosen for the

following discussion. In this work all performance plots are shown for various wave rotor pressure ratios indicating its effect on the performance enhancement.

Implementation Cases. There are several possibilities to top a gas turbine with a wave rotor. Considering possible design restrictions and preferences, five different advantageous implementation cases for a wave rotor into a given baseline engine can be introduced as follows:

Case A: same compressor, same turbine inlet temperature

Case B: same overall pressure ratio, same turbine inlet temperature

Case C: same combustor

Case D: same turbine

Case E: same compressor, same combustion end temperature

Case A: In Case A the pressure ratio of the compressor is kept unchanged, so the physical compressor of the baseline engine can also be used for the wave-rotor-enhanced engine provided the mass flow is kept approximately the same. The pressure in the combustion chamber of the enhanced engine is increased by the compression ratio of the wave rotor. This may require modifications to the structure of the combustion chamber and to the fuel injection system. The heat addition in the combustor is the same as for the baseline engine, but it takes place after the energy exchange in the wave rotor, hence the heat addition starts at a higher temperature. Thus, the combustion end temperature is even higher than that of the baseline engine, possibly requiring additionally a thermal enhancement of the combustor structure. The turbine of the topped engine might need to be adapted to efficiently utilize the higher pressure ratio. The turbine inlet temperature, however, is the same as that of the baseline engine. As will be shown later, this implementation case provides the highest thermal efficiency and specific work and the lowest value of *SFC*. However, concerns may be raised concerning emissions and combustor design due to the elevation of combustor pressure and temperature. Therefore, other topping cycles might be preferred which are discussed below.

Case B: In Case B the overall pressure ratio for the wave-rotor-enhanced engine is kept equal to that of the baseline engine, so that the combustor works under the same pressure. However, for the wave-rotor-topped engine, the heat addition in the combustor and the combustion end temperature are greater than those of the baseline engine. This may require some adaptation of the combustor, especially in the outlet region. The turbine and compressor work with lower pressure ratios, reducing the design challenges. Thus, both may be adapted advantageously. This might reduce the cost of the compressor and turbine due to reduction of stages in multistage types (mostly axial), or due to reduction of the tip diameter in radial types (mostly single-stage). With a smaller tip diameter the wheels can be manufactured more economically over a shorter time from cheaper materials with less strength and on smaller machines. Besides an attractive performance enhancement, this case additionally provides the highest turbine outlet temperature of all five cases investigated. The temperature of the leaving exhaust gas is much higher than that of the baseline engine. Therefore, this case is attractive for an external heat recovery application or for internal recuperation that can enhance the performance further.

Case C: Case C assumes that it is desirable for the wave-rotor-enhanced engine to use the unmodified combustor of the baseline engine. So the overall pressure ratio and combustor inlet and outlet temperatures for the wave-rotor-enhanced engine are kept equal to those of the baseline engine. The heat addition in the combustor is consequently the same.[1] The implementation of the wave rotor considerably reduces the pressure ratio of the turbine and compressor. The compressor pressure ratio is as low as in Case B, and the turbine pressure ratio and turbine inlet temperature are even lower than those in Case B. Thus, the turbine and compressor could be made from less thermally resistant material. Compared to the baseline engine, they also could be smaller and hence less expensive, as discussed in Case B. This might be the main implementation reason because unfortunately, but not surprisingly, the unambitious combustor constrains the performance enhancement. It is nearly negligible for the smaller C-30 engine and even negative for the C-60 engine.

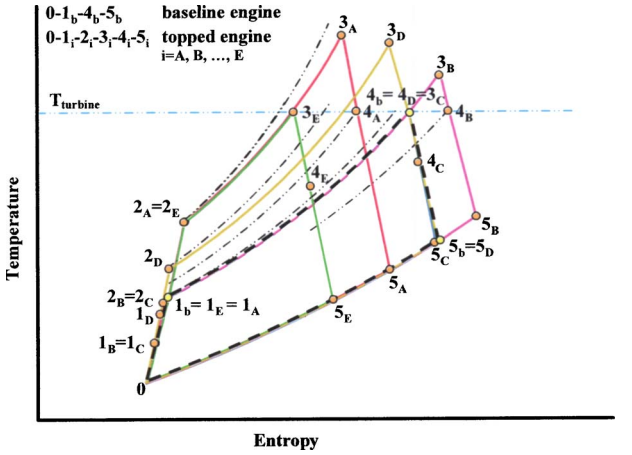

Fig. 5 Schematic T-s diagrams for a baseline cycle and five different wave-rotor-topped cycles

Case D: Case D employs the same physical turbine as the baseline engine. Due to the wave-rotor-topping, the compressor needs to produce a lower pressure ratio than that of the baseline engine. This allows for a smaller and less expensive compressor as discussed for Cases B and C. The pressure in the combustion chamber and the combustion end temperature are higher than those of the baseline engine, but lower than those of Case A. Hence, less effort might be required to adapt the structure and fuel injection of the combustion chamber. As a result of the lower pressure ratio in the compressor, hence lower compressor discharge temperature, the heat addition in the combustor has to be more than that for the baseline engine to utilize the same allowed turbine inlet temperature. This case gives the second highest performance increase for both baseline engines.

Case E: Case E is similar to Case A but the combustion end temperature (the cycle peak temperature) is restricted to the turbine inlet temperature of the baseline engine in order to avoid additional thermal requirements on the combustor design. The overall pressure ratio is the same as in Case A because this case employs the same physical compressor as for the baseline engine. Thus, the overall pressure ratio is greater than that of the baseline engine, by the wave rotor pressure ratio. The heat addition in the combustor is less than that for the baseline engine because to the wave rotor compression work is added to the fluid before combustion. The turbine in the topped cycle works with a slightly greater pressure ratio than the turbine of the baseline engine, but the turbine inlet temperature is less than that for the baseline engine. In fact, it is the lowest of all cases investigated. This may give the option to produce the turbine wheel at a lower cost out of less thermally resistant material.

According to the state numbering introduced in Fig. 2, Fig. 5 visualizes all five cases in schematic T-s diagrams. Path $0\text{-}1_b\text{-}4_b\text{-}5_b$ represents the baseline cycle and $0\text{-}1_i\text{-}2_i\text{-}3_i\text{-}4_i\text{-}5_i$ (i = A, B, C, D, E) indicates the wave-rotor-topped cycles, where the subscripts indicate the case. One of the five cases might be preferable for a practical design, however, intermediate design cases

[1]The wave rotor compression efficiency is greater than the compressor efficiency. Therefore, the combustor inlet temperature is in fact negligibly smaller and hence the heat addition is negligibly greater than that in the baseline engine.

are possible. In the following it is assessed how the wave-rotor-topping enhances the performance of C-30 and C-60 baseline gas turbine engines.

Analytical Procedure. According to state numbering introduced in Fig. 2, the following steps are taken to calculate the thermodynamic properties of the gases in different states of the topped cycle:

Path 0-1: Compressor. With the given compressor inlet temperature ($T_0=T_{t0}$), the compressor outlet total temperature and pressure are calculated from the adiabatic relations:

$$T_{t1} = T_{t0} + \frac{T_{t0}}{\eta_C}\left(\Pi_C^{\frac{\gamma_{air}-1}{\gamma_{air}}} - 1\right) \tag{1}$$

$$\frac{p_{t1}}{p_0} = \frac{p_{t1}}{p_{t0}} = \Pi_C \tag{2}$$

where the compressor isentropic efficiency (η_C) relates the compressor pressure ratio (Π_C) to the compressor polytropic efficiency (η_{PC}) through:

$$\eta_C = \frac{\Pi_C^{\frac{\gamma_{air}-1}{\gamma_{air}}} - 1}{\Pi_C^{\frac{\gamma_{air}-1}{\gamma_{air}\eta_{PC}}} - 1} \tag{3}$$

For Cases A and E, the compressor pressure ratio is equal to that of the baseline engine (e.g., for C-30 engine $\Pi_C=3.6$ and for C-60 engine $\Pi_C=4.8$). However, for Cases B and C its value is calculated by dividing the baseline compressor pressure ratio with the wave rotor compression ratio (PR_W). For Case E, the value of Π_C is calculated in a way that keeps the pressure at the turbine inlet equal for both baseline and topped engines. This calculation can be performed by inversely solving of Eqs. (1)–(21). The compressor specific work is obtained by:

$$w_C = Cp_{air}(T_{t1} - T_{t0}) = \frac{Cp_{air}T_{t0}}{\eta_C}(\Pi_C^{\frac{\gamma_{air}-1}{\gamma_{air}}} - 1) \tag{4}$$

Path 1-2: Compression in the Wave Rotor. The flow properties after the wave rotor compression process are obtained from the adiabatic relations similarly to those of the compressor:

$$T_{t2} = T_{t1} + \frac{T_{t1}}{\eta_{WC}}(PR_W^{\frac{\gamma_{air}-1}{\gamma_{air}}} - 1) \tag{5}$$

$$\frac{p_{t2}}{p_{t0}} = \frac{p_{t2}}{p_{t1}}\frac{p_{t1}}{p_{t0}} = PR_W \cdot \Pi_C \tag{6}$$

Path 2-3: Combustion Chamber. The value of fuel–air ratio ($f=m_f/m_{air}$) can be obtained by applying the energy (first law) equation to the combustion chamber:

$$\eta_Q\, f\, h_{PR} = (1+f)Cp_{gas}T_{t3} - Cp_{air}T_{t2} \tag{7}$$

where h_{PR}=43,000 kJ/kg is the heating value used for all calculations here. This equation gives f as:

$$f = \frac{Cp_{gas}T_{t3} - Cp_{air}T_{t2}}{\eta_Q\, h_{PR} - Cp_{gas}T_{t3}} \tag{8}$$

Alternatively, f can be expressed based on the turbine total inlet temperature (T_{t4}) and the compressor total exit temperature (T_{t1}). For this purpose, the wave rotor compression and expansion specific work (per unit mass of air flow) are defined, respectively, as follows:

$$w_{WC} = Cp_{air}(T_{t2} - T_{t1}) \tag{9}$$

$$w_{WE} = (1+f)Cp_{gas}(T_{t3} - T_{t4}) \tag{10}$$

Here, it is considered that $\dot{m}_1=\dot{m}_2=\dot{m}_{air}$ and $\dot{m}_3=\dot{m}_4=\dot{m}_{air}+\dot{m}_f$. Other cycles exist in which the mass flow rates $\dot{m}_1$ and $\dot{m}_2$ are not the same, and, correspondingly the mass flow rates $\dot{m}_3$ and $\dot{m}_4$ may not be equal either. These cycles are not considered here. Using Eqs. (9) and (10), Eq. (7) can be expressed as:

$$\eta_Q\, f\, h_{PR} = (1+f)Cp_{gas}T_{t4} + w_{WE} - w_{WC} - Cp_{air}T_{t1} \tag{11}$$

Because the net output work of the wave rotor is zero ($w_{WC}=w_{WE}$), solving for f leads to:

$$f = \frac{Cp_{gas}T_{t4} - Cp_{air}T_{t1}}{\eta_Q\, h_{PR} - Cp_{gas}T_{t4}} \tag{12}$$

For Cases C and E, T_{t3} is equal to the baseline inlet turbine temperature, therefore, Eq. (8) is used to calculate f. For Cases A, B, and D, where T_{t4} is a known value and is equal to the baseline inlet turbine temperature, f can be obtained from Eq. (12). The relation between T_{t3} and T_{t4} can be found by equating Eqs. (9) and (10):

$$T_{t3} = T_{t4} + \left[\frac{T_{t1}}{\eta_{WC}}(PR_W^{\frac{\gamma_{air}-1}{\gamma_{air}}} - 1)\right]\frac{Cp_{air}}{(1+f)Cp_{gas}} \tag{13}$$

Finally, the total pressure after the combustion chamber is obtained by:

$$\frac{p_{t3}}{p_{t0}} = \frac{p_{t3}}{p_{t2}}\frac{p_{t2}}{p_{t0}} = \Pi_{comb} \cdot PR_W \cdot \Pi_C \tag{14}$$

Path 3-4: Expansion in the Wave Rotor. To obtain the turbine inlet total pressure (p_{t4}), it is convenient to express the wave rotor compression work and the expansion work in terms of pressure ratios:

$$\dot{W}_{WC} = \dot{m}_{air}Cp_{air}(T_{t2} - T_{t1}) = \frac{\dot{m}_{air}Cp_{air}T_{t1}}{\eta_{WC}}(PR_W^{\frac{\gamma_{air}-1}{\gamma_{air}}} - 1) \tag{15}$$

$$\dot{W}_{WE} = (\dot{m}_{air}+\dot{m}_f)Cp_{gas}(T_{t3} - T_{t4}) = (\dot{m}_{air}+\dot{m}_f)Cp_{gas}\eta_{WE}T_{t3} \times\left[1 - \left(\frac{PO}{\Pi_{comb}PR_W}\right)^{\gamma_{gas}-1/\gamma_{gas}}\right] \tag{16}$$

where $PO=p_{t4}/p_{t1}$ is the gain pressure ratio across the wave rotor. Equating the compression work to the expansion work leads to:

$$\frac{Cp_{air}T_{t1}}{\eta_{WC}}(PR_W^{\frac{\gamma_{air}-1}{\gamma_{air}}} - 1) = (1+f)Cp_{gas}\eta_{WE}T_{t3} \times\left[1 - \left(\frac{PO}{\Pi_{comb}PR_W}\right)^{\gamma_{gas}-1/\gamma_{gas}}\right] \tag{17}$$

Substituting T_{t3} from Eq. (13) into Eq. (17) and some algebra gives:

$$PO = \Pi_{comb}PR_W\left\{1 - \frac{A\frac{1}{\eta_{WE}\eta_{WC}}B}{1 + A\frac{1}{\eta_{WC}}B}\right\}^{\gamma_{gas}/\gamma_{gas}-1} \tag{18}$$

where

$$A = \frac{Cp_{air}}{(1+f)Cp_{gas}} \tag{19}$$

$$B = \frac{T_{t1}}{T_{t4}}[PR_W^{(\gamma_{air}-1)/\gamma_{air}} - 1] \tag{20}$$

Equation (18) is a modified version of the "wave-rotor characteristic" equation introduced in the literature [14]. This equation represents the performance of the wave rotor. By using Eq. (18), the turbine inlet total pressure is obtained by:

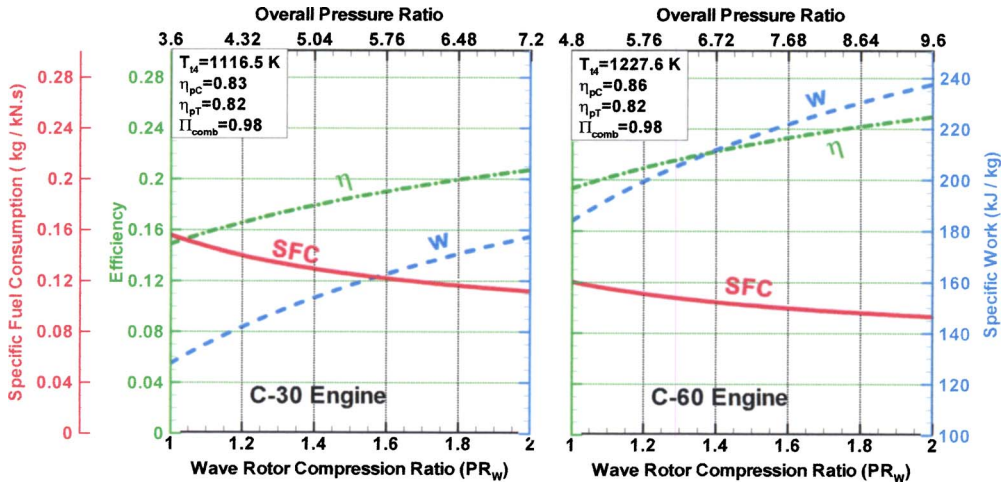

Fig. 6 Thermal efficiency, specific work, and *SFC* for the wave-rotor-topped engines versus the wave rotor pressure ratio and overall pressure ratio, Case A consideration

$$\frac{p_{t4}}{p_{t0}} = \frac{p_{t4}}{p_{t1}}\frac{p_{t1}}{p_{t0}} = PO \cdot \Pi_C \tag{21}$$

Path 3-4: Turbine. The turbine specific work (per unit mass of air flow) can be calculated knowing the pressure ratio across the turbine:

$$W_T = (1+f)Cp_{gas}(T_{t4} - T_{t5}) = (1+f)\eta_T Cp_{gas} T_{t4}\left[1 - \left(\frac{p_{t0}}{p_{t4}}\right)^{\frac{\gamma_{gas}-1}{\gamma_{gas}}}\right] \tag{22}$$

Assuming the turbine expands the hot gas leaving the wave rotor to atmospheric pressure ($p_{t5}=p_{t0}$). As a result, the total temperature of the gas leaving the turbine (T_{t5}) can be calculated from the above equation.

After calculating the thermodynamic properties of all states in the cycle, it is possible to calculate the engine performance parameters. The net specific output work produced by the engine can be calculated by subtracting the turbine specific work from the compressor work as $w=w_T-w_C$. With the amount of specific heat addition through the combustion process being defined as $q=f.h_{PR}$, the thermal efficiency can be written as $\eta=w/q$. Finally, the specific fuel consumption (*SFC*) is calculated by SFC=f/w.

Predicted Performance Results

Case A is the most common case discussed in the literature and it gives mostly the best performance enhancement. Therefore, it is discussed here in more details. Figure 6 illustrates the increase of cycle thermal efficiency (dash dot) and specific work (dashed), and the decrease of specific fuel consumption (solid) with increasing wave rotor pressure ratio PR_W for both C-30 and C-60 topped engines. The plot visualizes how the effect develops from the baseline engine with $PR_W=1$ until $PR_W=2$ which might be a practical limit for the investigated application. However, if the wave rotor pressure ratio increases beyond this limit, the trend already shows that the rate of increase of the effect diminishes while technical problems may increase. With a conceivable wave rotor pressure ratio of 1.8, the thermal efficiency of the baseline cycle increases from 14.9% to 20.0% for the C-30 engine and from 19.4% to 24.2% for the C-60 engine. Simultaneously, the specific work increases from 128 to 171 kJ/kg for the C-30 engine and from 184 to 231 kJ/kg for the C-60 engine. The specific fuel consumption (*SFC*) of the C-30 engine decreases from 0.156 to 0.116 kg/kN.s and it reduces from 0.120 to 0.095 kg/kN.s for the C-60 engine.

A better picture of the performance improvement is obtained by calculating the relative increases of thermal efficiency, specific work, and the relative decrease of *SFC* as shown in Fig. 7. For Case A, the relative increases of thermal efficiency and specific work (dash–dot) are precisely the same as it is obvious from $\eta=w/q$ where the heat addition $q=f.h_{PR}$ is the same for both topped and baseline engines. For a wave rotor pressure ratio of 1.8, Fig. 7 indicates an attractive relative performance improvement in thermal efficiency and specific work of about 33.8% and a 25.2% reduction in *SFC* (solid) for the C-30 engine. The C-60 engine shows a 25.1% enhancement in thermal efficiency and specific work and a 20.1% reduction in *SFC*.

More detailed documentation of these cases are not presented here. The reader is referred to Ref. [16]. Instead, numerical values of the predicted performance enhancement of all five investigated cases with a wave rotor pressure ratio of 1.8 are summarized in Table 2. In this table, Π_T represents the turbine pressure ratio. Subscript "gain" indicates the relative increase of thermal efficiency and specific work and decrease of *SFC*. Table 2 shows that Case A gives the highest performance increase for both baseline engines. After Case A, Case D gives the highest overall performance for the C-30 engine as for the C-60 engine. However, Case E provides the second highest thermal efficiency and the lowest *SFC* for the C-60 engine.

Figure 8 shows maps of the relevant design space for Cases A, B, and D for each engine. The only fixed parameters are turbine inlet temperature, the polytropic efficiencies of the compressor and turbine corresponding to the respective baseline engine, and the combustion chamber pressure loss as indicated in the upper-right hand corner legend of each map. Performance maps valid for Cases C and E of the C-30 and the C-60 engines are shown in Fig. 9 which have lower turbine inlet temperatures than that indicated in Fig. 8. Instead, Cases C and E have the same combustion end temperature as the baseline engine, as indicated in the upper-right hand corner of these maps.

The maps allow predicting the performance of the wave-rotor-enhanced engine in terms of thermal efficiency (green), specific work (blue), and *SFC* (red) for any combination of the compressor pressure ratio (abscissa) and the wave rotor pressure ratio PR_W (parameter labeled in black). In these maps, the multiplication of compressor pressure ratio p_{t1}/p_0 and wave rotor pressure ratio PR_W determines the overall cycle pressure ratio p_{t2}/p_0 (orange). The locus of optimum compressor pressure ratio points (for highest thermal efficiency and specific work at each achievable wave rotor pressure ratio) are connected by black solid lines. The optima for *SFC* are found at the same combination of the compres-

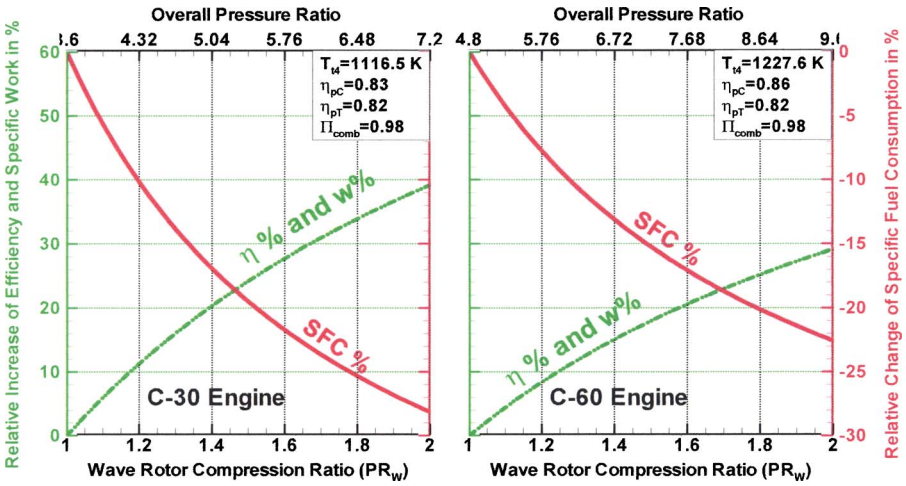

Fig. 7 Relative values of thermal efficiency, specific work, and SFC for the wave-rotor-topped engines versus the wave rotor pressure ratio and overall pressure ratio, Case A consideration

sor pressure ratio and PR_W as the optima of the thermal efficiency.

Such maps are not only very useful to explore the possible enhancement of already existing baseline engines, but they also serve well for selecting a design point or region for designing a new wave-rotor-topped engine. In all plots, the performance points of the baseline engine (PR_W=1) and the wave-rotor-enhanced engines of all cases with a wave rotor pressure ratio of PR_W=1.8 can be found. For instance in Fig. 8, starting from the performance point of the baseline engine, the performance values for Case A are found by moving vertically upwards (e.g., along the dashed line for constant compressor pressure ratio p_{t1}/p_0) until the corresponding performance curve of the expected wave rotor pressure ratio is crossed. Case B is found by moving along a line of constant overall pressure ratio p_{t2}/p_0 (orange).

The results indicate that for every compressor pressure ratio in each design space shown here, the performance of the topped engine is always higher than that of the corresponding baseline engine with the same compressor pressure ratio (Case A consideration). The increase of PR_W always increases the performance. However, for higher compressor pressure ratios the benefit of using a wave rotor progressively diminishes. In fact, for compressor pressure ratios greater than around 11, almost no benefit can be obtained for the C-30 engine. An identical statement applies to the C-60 engine for compressor pressure ratios above around 15. The benefit is clearly the greatest for lower compressor pressure ratios. This suggests that the wave-rotor-topping for microturbines with low compressor pressure ratios can produce the greatest relative benefit. Moreover, as expected and known for baseline engines (PR_W=1), it is also true for wave-rotor-topped engines that the compressor pressure ratio for the maximum specific work is always less than that of the maximum thermal cycle efficiency. However, with increasing wave rotor pressure ratio, the optima come closer together, while moving towards lower compressor pressure ratio. This can be viewed as an additional advantage for applying wave rotors to small gas turbines with low compressor pressure ratios. So as the plots show, adding a wave rotor with a 1.8 pressure ratio to C-30 or C-60 baseline engines with a compressor pressure ratio p_{t1}/p_0=3.6 or p_{t1}/p_0=4.8, respectively, already brings the design point into the optimum range for highest specific work and nearly half way closer to the optimum for highest thermal efficiency.

Table 2 Performance comparison between baseline engines and five cases of wave-rotor-topping with a wave rotor pressure ratio of 1.8

	Case A		Case B		Case C		Case D		Case E		Baseline	
Identical to baseline engine are:	• compressor • turbine inlet temp.		• overall press. ratio • turbine inlet temp.		• combustor		• turbine		• compressor • combustion end temp.			
	p_{t1}, T_{t1}, T_{t4}		$p_{t2}=p_{t1b}$, T_{t4}		$p_{t2}=p_{t1b}$, T_{t2}, T_{t3}		$P_{t2}=p_{t1b}$, p_{t4}, T_{t4}		P_{t1}, T_{t1}, $T_{t3}=T_{t4b}$			
Engines	C-30	C-60	C-30	C-60	C-30	C-60	C-30	C-60	C-30	C-60	C-30	C-60
T_{t4} [K]	1116	1228	1116	1228	1044	1149	1116	1228	1027	1132	1116	1228
q [kJ/kg]	855	952	946	1047	857	950	894	993	747	833	855	952
Π_C	3.60	4.80	2.00	2.67	2.00	2.67	2.84	3.77	3.60	4.80	3.60	4.80
Π_T	4.38	5.87	2.60	3.48	2.55	3.41	3.53	4.70	4.24	5.70	3.53	4.70
w_C [kJ/kg]	167	206	81	116	81	116	131	167	167	206	167	206
w_T [kJ/kg]	338	437	231	324	211	298	295	391	305	396	295	391
w [kJ/kg]	**171**	**231**	**150**	**208**	**130**	**182**	**165**	**224**	**137**	**190**	**128**	**184**
SFC[kg/kN.s]	**0.116**	**0.095**	**0.147**	**0.117**	**0.153**	**0.121**	**0.126**	**0.103**	**0.126**	**0.102**	**0.156**	**0.120**
η	**0.200**	**0.242**	**0.158**	**0.199**	**0.151**	**0.192**	**0.184**	**0.225**	**0.184**	**0.227**	**0.149**	**0.194**
$(w)_{gain}$ [%]	**33.8**	**25.1**	**17.1**	**13.0**	**1.7**	**-1.1**	**29.1**	**21.5**	**7.7**	**2.9**		
$(SFC)_{gain}$ [%]	**25.2**	**20.1**	**5.5**	**2.6**	**1.4**	**-0.8**	**19.0**	**14.1**	**18.9**	**14.9**		
$(\eta)_{gain}$ [%]	**33.8**	**25.1**	**5.9**	**2.7**	**1.5**	**-1.8**	**23.5**	**16.5**	**23.4**	**17.5**		

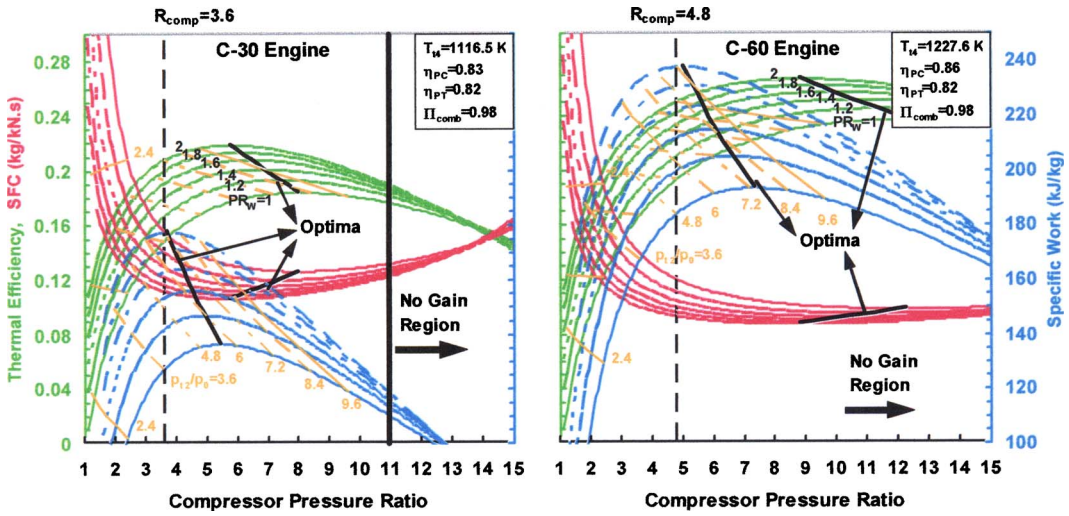

Fig. 8 Performance map for wave-rotor-topping of gas turbines, Cases A, B, and D

Comparison Between Adding a Second Compressor Stage and Wave-Rotor-Topping. The wave-rotor-topping competes mainly against adding a second compressor stage to the single stage baseline engine. In this competition one major advantage of the wave-rotor-topping is that the wave rotor favorably operates mechanically independently from the high-speed engine shaft. Therefore, adding a retrofit wave rotor does not require the redesign of the challenging dynamic system. Even if the compressor or turbine wheel is adapted subsequently to utilize the full potential of the wave-rotor-topping, the dynamic system may change but not as dramatically as if a second compressor stage was added. Thus, by default the wave rotor is a system for achieving similar thermodynamic advantages as by adding a second compressor stage or a high pressure spool, but with many fewer dynamic challenges.

To justify the wave-rotor-topping approach further, the performance results of both competing solutions are compared below. For the addition of a second compressor stage, performance data are calculated for the five most probably relevant pressure ratios of the second stage described here:

$$\Pi_{c2} = \mathrm{PR}_W.$$

A (perhaps) logical way to compare both systems would be to assume the same compression ratio for the second compressor stage as for the wave rotor. Hence the compression ratio of the second compressor stage would be $\Pi_{c2}=1.8$, because the assumed wave rotor compression ratio is $PR_W=1.8$.

$$w_{C2} = w_{C1}$$

More likely, when the effort of adding a second compressor stage is undertaken, the designer would not limit the pressure ratio of the second stage to $\Pi_{C2}=1.8$. It might be desired to a add second compressor wheel that is similar to the existing first stage (or the same) for reasons such as using existing experience, or producing both wheels cost effectively as identical wheels, or producing them geometrically similar using the same or slightly modified tools. This approach can be modeled by setting the compressor shaft work of the second stage equal to that of the first stage, simulating the same angular momentum change of the flow in both stages at the same shaft. Because the inlet air temperature for the second stage is much higher, the pressure ratio of the second stage is less than that of the first stage $\Pi_{C2} < \Pi_{C1}$.

$$\Pi_{C2} = \Pi_C$$

Alternatively, it could simply be assumed that the pressure ratio of the second stage is equal to the pressure ratio in the first stage. This is a common design approach.

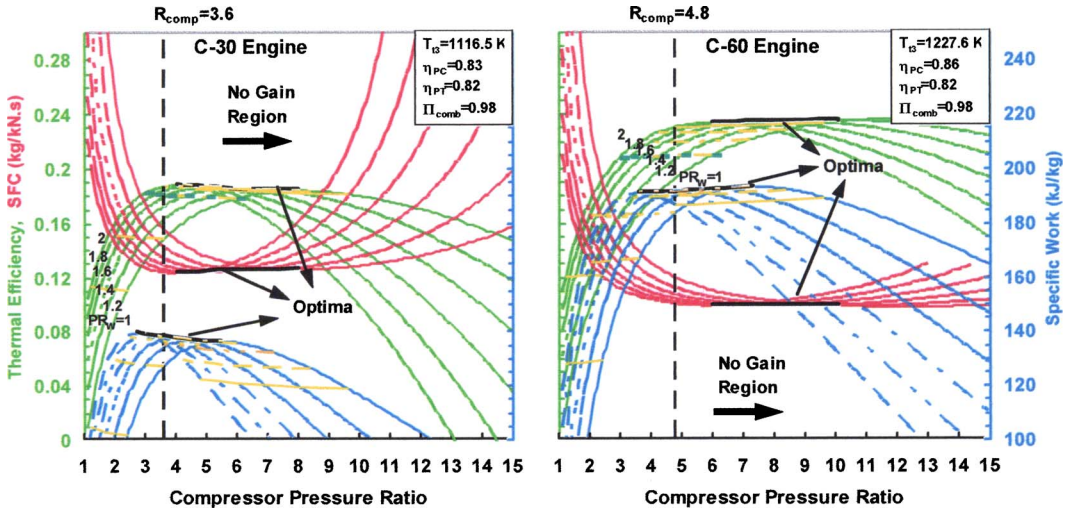

Fig. 9 Performance map for wave-rotor-topping of gas turbines, Cases C and E

Table 3 Performance comparison between adding a conventional second compressor stage and wave-rotor-topping Cases A and E with a wave rotor pressure ratio of 1.8; baseline engine C-30

C-30	Two-Stage Compressor					Wave Rotor Topped		Baseline
Feature	$\Pi_C(w)_{opt.}$	$\Pi_{C2}=PR_W$	$\Pi_C(\eta)_{opt.}$	$w_{C2}=w_{C1}$	$\Pi_{C2}=\Pi_{C1}$	Case **A**	Case **E**	
Π_{C2}	1.52	1.8	2.22	2.42	3.6	1.8	1.8	
w [kJ/kg]	136	135	129	125	95	171	137	128
SFC[kg/kN.s]	0.133	0.128	0.126	0.127	0.141	0.116	0.126	0.156
η	0.175	0.181	0.184	0.183	0.164	0.200	0.184	0.149
$(w)_{gain}$ [%]	6.3	5.5	0.8	-2.3	-25.8	33.8	7.7	
$(SFC)_{gain}$ [%]	14.5	17.9	18.9	18.6	9.6	25.2	18.9	
$(\eta)_{gain}$ [%]	17.5	21.5	23.4	22.8	10.1	33.8	23.4	

$\Pi_C(w_{\text{net}})_{\text{opt.}}$ and $\Pi_C(\eta)_{\text{opt.}}$

It might be desirable to compare the wave-rotor-topped engine with a two-stage compressor engine that has an overall pressure ratio $\Pi_{C2}\cdot\Pi_{C1}$ corresponding to the optimum for maximum specific work $\Pi_C(w)_{\text{opt}}$ or the optimum for maximum efficiency $\Pi_C(\eta)$opt.. The resulting values for specific work and thermal efficiency, respectively, are the maximum values actually obtainable by enhancing the pressure ratio of a conventional compressor. The values of $\Pi(w)_{\text{opt}}$ and $\Pi(\eta)_{\text{opt}}$ can be found by using performance maps in Figs. 8 and 9 and following the curves for $PR_W=1$ to their optimum points.

In all performance calculations above, it is assumed that the polytropic compression efficiency of the second stage is equal to that of the single stage baseline compressor The performance values of all these two-stage-compressor cases as well as intermediate cases can also be read off the performance maps in Figs. 8 and 9 following the curves for $PR_W=1$. The compressor pressure ratio at the abscissa then corresponds to the overall pressure ratio $\Pi_{C2}\cdot\Pi_{C1}$.

The performance results are compiled for the C-30 engine in Table 3 and for the C-60 engine in Table 4 for all five two-stage-compressor cases described above. The two-stage-compressor engines are compared with the wave-rotor-topped engine Case A and Case E. These cases are more suitable to be compared with two-stage-compressor engines for a few reasons. Both cases employ the same compressor as the first stage of the baseline engines. Case A has shown the highest performance improvement and it represents the maximum performance achievable for a wave-rotor-topping cycle. In Case E, the baseline compressor is the same and the combustion end temperature is the same as for the baseline engine (not requiring any thermal enhancement of the combustor). It can be understood that this is exactly the case for the two-stage-compressor engine, where the combustion end temperature is simultaneously the turbine inlet temperature (which is never the case for wave-rotor-topping). The two-stage-compressor values may also be compared with the wave-rotor-topping Cases B, C, and D using the supplied data in Table 2.

Tables 3 and 4 show that the gain in predicted overall efficiency, specific shaft work, and *SFC* of the wave-rotor-topped engine in Case A is always greater than any obtainable values for the two-stage-compressor engine. A look at the maps in Fig. 8 easily verifies this for the relevant design space. In Fig. 8 the performance points for Case A lie well above any point at the curves for $PR_W=1$ where all the performance data of the two-stage-compressor engine can be found. For the C-30 engine, Case E in Table 3 still shows a higher performance than any two-stage-compressor configuration. For the C-60 engine, however, Case E in Table 4 achieves nearly the same performance as a two-stage-compressor engine with a second-stage compression ratio in the range between the two optima for maximum specific work and maximum overall efficiency (minimum *SFC*), $\Pi_{C2}=1.52,\ldots,2.55$. Finally, the results show again that the compressor pressure ratio for the maximum specific work is always less than that of the maximum overall cycle efficiency (minimum *SFC*).

Besides the drawbacks of the two-stage-compressor implementation already mentioned, a second compressor stage adds not only a second compressor wheel, it always requires an enhanced combustor capable for higher combustion pressure and a turbine adapted to considerably higher pressure ratio. Finally, it requires an enhanced engine shaft, transmitting much more compression work. Quite opposite for the wave-rotor-enhanced engine, the transmitted compression work for all considered wave-rotor-topping cases is always either less (Cases B, C, D) or the same as for the baseline engine (Cases A and D). The combustion pressure ratio can be kept the same (Cases B and C). Furthermore, the

Table 4 Performance comparison between adding a conventional second compressor stage and wave-rotor-topping Cases A and E with a wave rotor pressure ratio of 1.8; baseline engine C-60

C-60	Two-Stage Compressor					Wave Rotor Topped		Baseline
Feature	$\Pi_C(w)_{opt.}$	$\Pi_{C2}=PR_W$	$\Pi_C(\eta)_{opt.}$	$w_{C2}=w_{C1}$	$\Pi_{C2}=\Pi_{C1}$	Case **A**	Case **E**	
Π_{C2}	1.52	1.8	2.55	2.79	4.8	1.8	1.8	
w [kJ/kg]	193	192	179	173	118	231	190	184
SFC[kg/kN.s]	0.105	0.101	0.098	0.098	0.115	0.095	0.102	0.120
η	0.222	0.229	0.236	0.236	0.203	0.242	0.227	0.194
$(w)_{gain}$ [%]	4.9	4.3	-2.7	-6.0	-35.9	25.1	2.9	
$(SFC)_{gain}$ [%]	12.5	15.8	18.3	18.3	4.2	20.1	14.9	
$(\eta)_{gain}$ [%]	14.4	18.0	21.6	21.6	4.6	25.1	17.5	

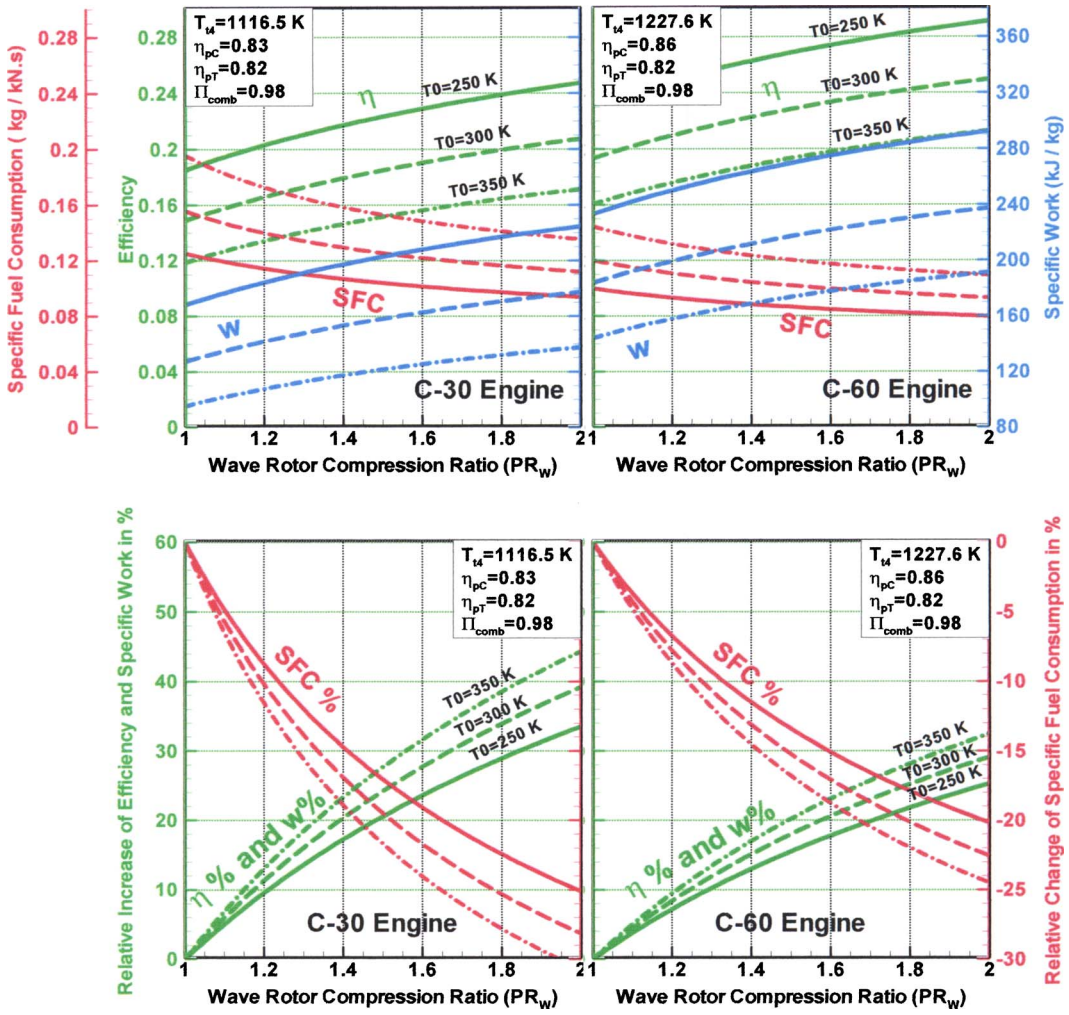

Fig. 10 Effect of ambient temperature-overall thermal efficiency, specific work, and specific fuel consumption versus wave rotor pressure ratio and overall pressure ratio for Case A

pressure ratio that has to be accommodated in the turbine is always less for the wave-rotor-topped engine than for the two-stage-compressor engine with the same or greater overall pressure ratio, causing likely fewer problems when adapting the turbine. For the wave-rotor-topping Cases B and C, the turbine pressure ratio is even less than that of the single stage baseline engine. Additionally, in Cases C and E the wave-rotor-topping even lowers the turbine inlet temperature, which allows the designer to use a turbine made of a lower cost material.

Effect of Compressor Inlet Temperature. It is well known that the performance of gas turbines is affected by varying ambient conditions [58]. For instance, both thermal efficiency and output power of a gas turbine engine with a fixed turbine inlet temperature decrease when the compressor inlet temperature rises. This is disadvantageous if a stationary gas turbine is installed in hot-weather locations. Under this consideration, it is proved in the following that for such conditions the wave-rotor-topping is even more advantageous.

For simulation, it is assumed that the compressor isentropic efficiency stays constant although a slight decrease might be expected. It is furthermore assumed that the specific compression work stays constant since the compressor geometry does not change. Hence, the compressor pressure ratio decreases by increasing ambient temperature due to basic thermodynamics. For the baseline engine it is obvious this results in a lower turbine pressure ratio and less specific work produced by the engine.

The performance values of the wave-rotor-enhanced engines of Cases A and B, which are the most considered cases discussed in the literature, for compressor inlet temperatures of 250, 300, and 350 K are shown in Figs. 10 and 11, respectively, for a range of wave rotor compression ratios $PR_W = 1, \ldots, 2$.

For the wave-rotor-enhanced engines, the general performance trend is the same as baseline engines. However, while the absolute performance degrades at higher ambient temperatures for baseline and topped engines, performance gains of the enhanced engines relative to the baseline engines increase, making this technology even more desirable for applications under hot-weather conditions. This reversed effect is visualized in the figures especially in the lower part showing the relative gains of the topped engines.

Wave Rotors for Gas Turbines with Recuperations. Figure 12 shows a block diagram of a recuperated gas turbine topped with a four-port wave rotor. The wave rotor is placed after the compressor and before the recuperator. Figure 13 shows a schematic T-s diagram of the baseline engine and the corresponding wave-rotor-topped engine for Cases A and B. Path $0\text{-}1_b\text{-}2_b^*\text{-}4_b\text{-}5_b\text{-}5_b^*$ represents the baseline cycle and path $0\text{-}1_i\text{-}2_i\text{-}2_i^*\text{-}3_i\text{-}4_i\text{-}5_i\text{-}5_i^*$ (i=A and B) indicates the wave-rotor-topped cycles. Only Cases A and B are considered in this study due to their high potential for performance improvement under recuperated conditions. All calculations have been presented only for the C-30 engine, while the conclusions are valid for the C-60 engine, too.

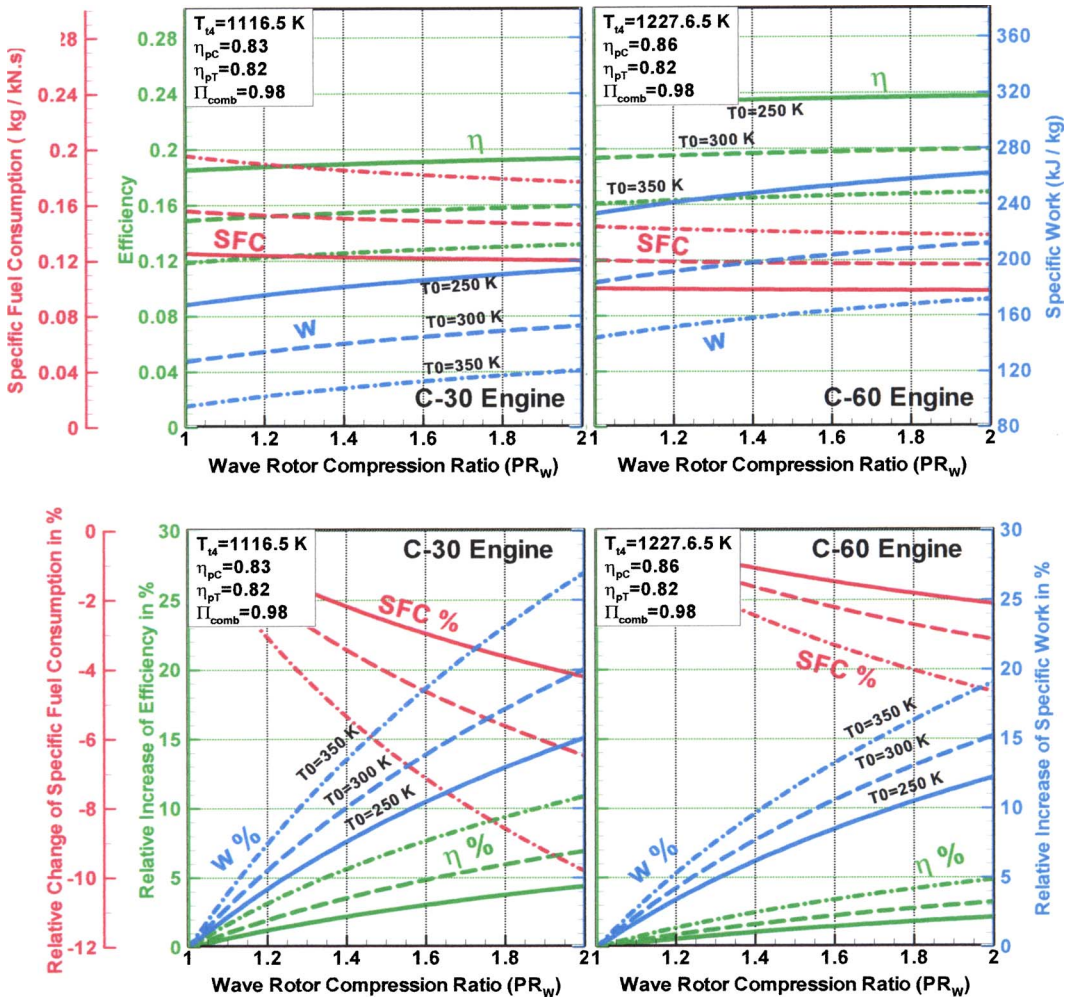

Fig. 11 Effect of ambient temperature-overall thermal efficiency, specific work, and specific fuel consumption versus wave rotor pressure ratio and overall pressure ratio for Case B

The analytical approach to analysis such wave-rotor-topped recuperated cycles has been introduced by the authors in previous work [59] and is not stated here. Instead, Table 5 summarizes the obtained results and shows a comparison between performance improvements of the simple and recuperated engines for implementations of both Cases A and B. It is seen from the table that the baseline engine (C-30 without the wave rotor) with recuperation has much higher efficiency (about twice) and lower *SFC* than those of the unrecuperated baseline engine due to the reduction of heat addition in the combustion process, as expected. As explained before, implementation of Case A into the baseline engine results in a significant performance improvement of the unrecuperated engine, however, the thermal efficiency and *SFC* improve-

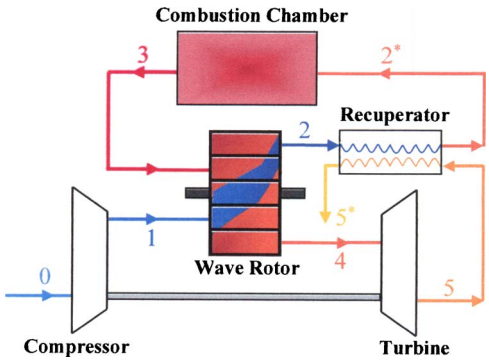

Fig. 12 Schematic of a recuperated gas turbine topped by a four-port wave rotor

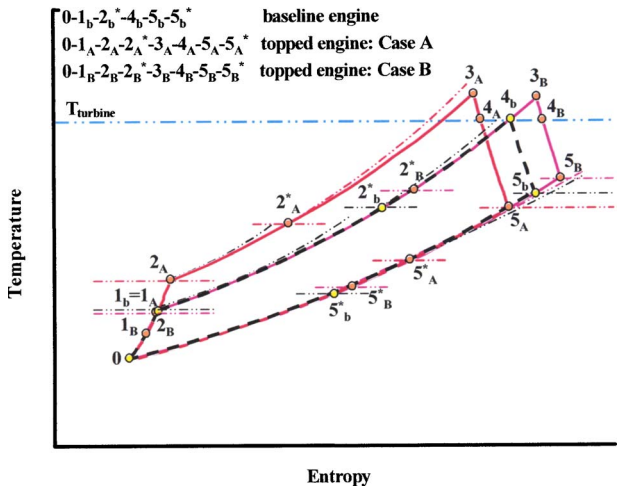

Fig. 13 Schematic T-s diagram for a recuperated baseline cycle and two wave-rotor-topped cycles

Table 5 Performance comparison between simple and recuperated engines and two cases of wave-rotor-topping with a wave rotor pressure ratio of 1.8, C-30 engine

	Case A		Case B		Baseline	
Engines	Simple	Recuperated	Simple	Recuperated	Simple	Recuperated
Π_C	3.60	3.60	2.00	2.00	3.60	3.60
Π_T	4.38	4.19	2.60	2.49	3.53	3.39
q [kJ/kg]	855	603	946	505	855	470
w_C [kJ/kg]	167	167	81	81	167	167
w_T [kJ/kg]	338	328	231	219	295	284
w [kJ/kg]	**171**	**161**	**150**	**138**	**128**	**117**
SFC [kg/kN.s]	**0.116**	**0.087**	**0.147**	**0.085**	**0.156**	**0.094**
η	**0.200**	**0.266**	**0.158**	**0.273**	**0.149**	**0.248**
$(w)_{gain}$ [%]	**33.8**	**37.6**	**17.1**	**18.0**		
$(SFC)_{gain}$ [%]	**25.2**	**6.7**	**5.5**	**8.7**		
$(\eta)_{gain}$ [%]	**33.8**	**7.2**	**5.9**	**9.7**		

ments of the recuperated engine are much less than that of the specific work. In Case B, however, the topped recuperated cycle has higher performance compared to the unrecuperated engine and its thermal efficiency and *SFC* gains are even more than those of Case A. Case B takes advantage of the fact that the temperature difference between the air and the gas entering the recuperator of the topped engine ($T_{t5B}-T_{t2B}$) is more than that of Case A ($T_{t5A}-T_{t2A}$). This results in a higher recuperation effect for Case B. The results clearly demonstrate the advantage of implementing Case A for unrecuperated engines and implementing Case B for recuperated engines. The results also indicate that the recuperator enhances thermal efficiency and *SFC* better, while the wave-rotor is mostly better for enhancing the specific work output. Therefore, substituting a recuperator with a wave rotor may be guided by a preference for high power output and reduced unit cost, considering that a recuperator contributes about 25%–30% to the unit cost [11–13] and a wave rotor may be cheaper.

Conclusion

For the implementation of a wave rotor into two simple-cycle microturbines C-30 and C-60, the present investigation predicts an attractive performance enhancement for both baseline engines. The smaller C-30 engine would benefit more from the wave-rotor-topping than the C-60 engine. The C-30 engine overall efficiency and specific work may increase by up to 34% and for the C-60 engine by up to 25%. Five different cases of implementing a wave rotor into the existing baseline engines are investigated. Ideally, one of the three main components (compressor, combustor, or turbine) would remain unchanged when a wave rotor is implemented. However, compromises may be considered for tests or cost-effective prototype development, keeping two or even all three main components unchanged. Case A, in which the baseline compressor remains completely unchanged, appears to be the most beneficial case. However, the combustor works under higher pressure and with higher combustion end temperature. The turbine pressure ratio increases as well. Thus, an adaptation of the turbine wheel may be desired to utilize the obtained potential optimally. Other cases with unchanged overall pressure ratio (Cases B and C), with unchanged combustion end temperature (Cases D and E) or unmodified turbine (Case D) are investigated as well. Case B gives an increased turbine exit temperature and is therefore especially attractive for external heat recovery applications or internal recuperation, which would enhance the performance even more. Sacrificing some performance enhancement, the wave-rotor implementation can yield other advantages like decreased turbine inlet temperature (Cases C and E), reduced compressor pressure ratio (Cases B, C, and D) or reduced turbine pressure ratio (Cases B and C), which can reduce the gas turbine cost. Further, adding a wave rotor instead of a second compressor stage results in better or similar performance enhancement and has many other advantages. While a second compressor stage alters the dynamic system tremendously and always increases the combustion pressure, turbine inlet pressure and compressor work transmitted through the shaft, a wave-rotor implementation requires no or only minor changes to the dynamic system of the gas turbine spool. It can keep the combustion pressure the same, can even reduce the turbine inlet pressure or temperature and the transmitted shaft work for the compressor. Furthermore, it is shown that the performance degradation at higher temperatures is much less for the wave-rotor-topped engines than for the baseline engines, making this technology even more desirable for applications under hot-weather conditions. Finally, it is shown that the recuperator is better for improving overall thermal efficiency and specific fuel consumption, while the wave-rotor-topping is better for increasing the specific work output. Cost considerations may additionally favor the wave-rotor.

Acknowledgment

The authors wish to acknowledge the cooperation of Capstone Turbine Corporation, providing the baseline engine data. The assistance of A. Behinfar in sketching Figs. 1 and 3 is acknowledged.

References

[1] Craig, P., 1997, "The Capstone Turbogenerator as an Alternative Power Source" SAE Paper 970292.
[2] Kang, Y., McKeirnan, R., 2003, "Annular Recuperator Development and Performance Test for 200 kW Microturbine" ASME Paper GT-2003-38522.
[3] Benini, E., Toffolo, A., and Lazzaretto, A., 2003, "Centrifugal Compressor of A 100 KW Microturbine: Part 1-Experimental and Numerical Investigations on Overall Performance" ASME Paper GT2003-38152.
[4] Zauner, E., Chyou, Y. P., Walraven, F., and Althaus, R., 1993, "Gas Turbine Topping Stage Based on Energy Exchangers: Process and Performance" ASME Paper 93-GT-58.
[5] Rogers, C., 2003, "Some Effects of Size on the Performance of Small Gas Turbine" ASME Paper GT2003-38027.
[6] Shi, J., Venkata, R., Vedula, J. H., Connie, E. B., Scott, S. O., Bertuccioli, L., and Bombara, D. J., 2002, "Preliminary Design of Ceramic Components for the ST5+ Advanced Microturbine Engine" ASME Paper GT-2002-30547.
[7] Walsh, C., An, C., Kapat, J. S., and Chow, L. C., 2002, "Feasibility of a High-Temperature Polymer-Derived-Ceramic Turbine Fabricated Through Micro-Stereolithography" ASME Paper GT-2002-30548.
[8] McDonald, C. F., 1996, "Heat Recovery Exchanger Technology for Very Small Gas Turbine" Journal of Turbo and Jet Engines, **13**, pp. 239–261.
[9] Proeschel, R. A., 2002, "Proe 90TM Recuperator for Microturbine Applications" ASME Paper GT-2002-30406.
[10] Carman, B. G., Kapat, J. S., Chow, L. C., and An, L., 2002, "Impact of a Ceramic Microchannel Heat Exchanger on a Microturbine" ASME Paper GT2002-30544.
[11] McDonald, C. F., 2000, "Low Cost Recuperator Concept for Microturbine Applications" ASME Paper GT2000-167.
[12] Utriainen, E., and Sunden, B., 2001, "A Comparison of Some Heat Transfer Surfaces for Small Gas Turbine Recuperators" ASME Paper GT2001-0474.
[13] Maziasz, P. J., Pint, B. A., Swindeman, R. W., More, K. L., and Lara-Curzio,

E., 2003, "Selection, Development and Testing of Stainless Steel and Alloys for High-Temperature Recuperator Applications" ASME Paper GT2003-38762.
[14] Wilson, J. and Paxson, D. E., 1993, "Jet Engine Performance Enhancement Through Use of a Wave-Rotor Topping Cycle" NASA TM-4486.
[15] Fatsis A., and Ribaud Y., 1999, "Thermodynamic Analysis of Gas Turbines Topped with Wave Rotors" Aerosp. Sci. Technol., **3**, No. 5, pp. 293–299.
[16] Akbari, P., and Müller, N., 2003, "Performance Improvement of Small Gas Turbines Through Use of Wave Rotor Topping Cycles" ASME Paper GT2003-38772.
[17] Akbari, P., and Müller, N., 2003, "Performance Investigation of Small Gas Turbine Engines Topped with Wave Rotors" AIAA Pap. 2003-4414.
[18] Meyer, A., 1947, "Recent Developments in Gas Turbines" Chin. J. Mech. Eng., **69**, No. 4, pp. 273–277.
[19] Real, R., 1946, "The 3000 kW Gas Turbine Locomotive Unit" Brown Boveri Rev., **33**, No. 10, pp. 270-271.
[20] Meyer, A., 1947, "Swiss Develop New Gas Turbine Units" Electr. World, **127**, pp. 38-40.
[21] Azoury P. H., 1992, *Engineering Applications of Unsteady Fluid Flow*, John Wiley and Sons, New York.
[22] Rose, P. H., 1979, "Potential Applications of Wave Machinery to Energy and Chemical Processes" *Proceedings of the 12th International Symposium on Shock Tubes and Waves*, pp. 3–30.
[23] Seippel, C., 1940, Swiss Patent No. 225426.
[24] Seippel, C., 1942, Swiss Patent No. 229280.
[25] Seippel, C., 1946, "Pressure Exchanger" US Patent 2399394.
[26] Seippel, C., 1949, "Gas Turbine Installation" US Patent 2461186.
[27] Taussig, R. T., Hertzberg, A., 1984, "Wave Rotors for Turbomachinery" *Winter Annual Meeting of the ASME*, edited by Sladky, J. F., Machinery for Direct Fluid-Fluid Energy Exchange, AD-07, pp. 1–7.
[28] Zehnder, G., Mayer, A. and Mathews, L., 1989, "The Free Running Comprex®" SAE Paper 890452.
[29] Mayer, A., Oda, J., Kato, K., Haase, W. and Fried, R., 1989, "Extruded Ceramic-A New Technology for the Comprex® Rotor" SAE Paper 890453.
[30] Hiereth, H., 1989, "Car Tests With a Free-Running Pressure-Wave Charger-A Study for an Advanced Supercharging System" SAE Paper 890 453.
[31] Azoury, P. H., 1965-66, "An Introduction to the Dynamic Pressure Exchanger" Proc. Inst. Mech. Eng., **180**, Part 1, No. 18, pp. 451–480.
[32] Guzzella, L., Wenger, U., and Martin, R., 2000, "IC-Engine Downsizing and Pressure-Wave Supercharging for Fuel Economy" SAE Paper 2000-01-1019.
[33] Shreeve, R. P., Mathur, A., 1985, *Proceeding ONR/NAVAIR Wave Rotor Research and Technology Workshop*, Report NPS-67-85-008, Naval Postgraduate School, Monterey, CA.
[34] Paxson, D. E., 1992, "A General Numerical Model for Wave-Rotor Analysis" NASA TM-105740.
[35] Paxson, D. E., 1996, "Numerical Simulation of Dynamic Wave Rotor Performance" J. Propul. Power, **12**, No. 5, pp. 949-957.
[36] Welch, G. E., Jones, S. M., and Paxson, D. E., 1997, "Wave Rotor-Enhanced Gas Turbine Engines" J. Eng. Gas Turbines Power, **119**, No. 2, pp. 469–477.
[37] Welch, G. E., 1997, "Macroscopic Balance Model for Wave Rotors" J. Propul. Power, **13**, No. 4, pp. 508–516.
[38] Welch, G. E., 1997, "Two-Dimensional Computational Model for Wave Rotor Flow Dynamics" J. Eng. Gas Turbines Power, **119**, No. 4, pp. 978–985.
[39] Wilson, J., and Paxson, D. E., 1996, "Wave Rotor Optimization for Gas Turbine Topping Cycles" J. Propul. Power, **12**, No. 4, pp. 778–785. See SAE Paper 951411, and NASA TM 106951.
[40] Welch, G. E., 2000, "Overview of Wave-Rotor Technology for Gas Turbine Engine Topping Cycles" *Novel Aero Propulsion Systems International Symposium, The Institution of Mechanical Engineers*, pp. 2–17.
[41] Wilson, J., 1997, "Design of NASA Lewis 4-Port Wave Rotor Experiment" AIAA Pap. 97-3139. Also NASA CR-202351.
[42] Wilson J., and Fronek, D., 1993, "Initial Results from the NASA-Lewis Wave Rotor Experiment" AIAA Pap. 93-2521. Also NASA TM-106148.
[43] Wilson, J., 1997, "An Experiment on Losses in a Three Port Wave-Rotor" NASA CR-198508.
[44] Wilson, J., 1998, "An Experimental Determination of Loses in a Three-Port Wave Rotor" J. Eng. Gas Turbines Power, **120**, pp. 833–842. Also ASME Paper 96- GT-117, and NASA CR-198456.
[45] Paxson, D. E., 1993, "A Comparison Between Numerically Modeled and Experimentally Measured Loss Mechanisms in Wave Rotors" AIAA Pap. 93-2522.
[46] Paxson, D. E., 1995, "Comparison Between Numerically Modeled and Experimentally Measured Wave-Rotor Loss Mechanism" J. Propul. Power, **11**, No. 5, pp. 908–914. Also NASA TM-106279.
[47] Paxson D. E., and Wilson, J., 1995, "Recent Improvements to and Validation of the One Dimensional NASA Wave Rotor Model" NASA TM-106913.
[48] Paxson, D. E., and Nalim, M. R., 1999, "Modified Through-Flow Wave-Rotor Cycle with Combustor Bypass Ducts" J. Propul. Power, **15**, No. 3, pp. 462-467. Also AIAA Paper 97-3140, and NASA TM-206971.
[49] Nalim, M. R., and Paxson, D. E., 1999, "Method and Apparatus for Cold-Gas Reinjection in Through-Flow and Reverse-Flow Wave Rotors" US Patent 5,894,719.
[50] Jones, S. M., and Welch, G. E., 1996, "Performance Benefits for Wave Rotor-Topped Gas Turbine Engines" ASME Paper 96-GT-075.
[51] Weber, H. E., 1986, "Shock-Expansion Wave Engines: New Directions for Power Production" ASME Paper 86-GT-62.
[52] Weber, H. E., 1995, *Shock Wave Engine Design*, John Wiley and Sons, New York.
[53] Akbari, P., Kharazi, A. A., and Müller, N., 2003, "Utilizing Wave Rotor Technology to Enhance the Turbo Compression in Power and Refrigeration Cycles" ASME Paper IMECE2003-44222.
[54] Gyarmathy, G., 1983, "How Does the Comprex Pressure-Wave Supercharger Work?" SAE Paper 830234.
[55] Kentfield, J. A. C., 1993, *Nonsteady, One-Dimensional, Internal, Compressible Flows*, Oxford University Press, Oxford.
[56] Taussig, R. T., 1984, "Wave Rotor Turbofan Engines for Aircraft" *Winter Annual Meeting of the ASME*, edited by Sladky, J. F., Machinery for Direct Fluid-Fluid Energy Exchange, AD-07, pp. 9–45.
[57] Welch, G. E., 1996, "Two-Dimensional Computational Model for Wave Rotor Flow Dynamics" ASME Paper 96-GT-550.
[58] El Hadik, A. A., 1990, "The Impact of Atmospheric Conditions on Gas Turbine Performance" J. Eng. Gas Turbines Power, **112**, No. 4, pp. 590–595.
[59] Akbari, P., Müller, N., and Nalim, M. R., 2004, "Performance Improvement of Recuperated and Unrecuperated Microturbines Using Wave Rotor Machines," 2004 ASME-ICED Spring Technical Conference, Japan.